

Instrumented ultramicrohardness testing on NiTi alloys produced by selective laser melting

Danilo Abílio Corrêa Gonçalves ^{1*} 

Naiara Vieira Le Senéchal ¹ 

Fábio Silva de Oliveira ¹ 

Rafael Ramos ¹ 

Rodolfo da Silva Teixeira ² 

Paulo Paiva Oliveira Leite Dyer ³ 

Getúlio de Vasconcelos ⁴ 

Andersan dos Santos Paula ¹ 

Abstract

Nickel-titanium (NiTi) alloys, known for their shape memory effect and superelasticity, are distinguished by their shape recovery capabilities and corrosion resistance. In recent years, additive manufacturing (AM), especially selective laser melting (SLM), has gained prominence in the production of complex NiTi structures. This study employs instrumented ultramicrohardness testing to characterize the mechanical properties of these alloys, including Vickers hardness (HV), elastoplastic Vickers dynamic hardness (DHV-1), plastic Vickers dynamic hardness (DHV-2), and indentation modulus (E_{it}). The tests were conducted on NiTi samples produced by SLM, with a laser remelting procedure applied. The results indicate a decreasing trend in HV, DHV-1, and DHV-2 values with increasing energy density in SLM fabrication, suggesting greater formation of matrix phases (B2, B19', and R) and a lower percentage of Ni_xTi_y intermetallic precipitates.

Keywords: Selective laser melting; Additive manufacturing; NiTi; Ultramicrohardness.

1 Introduction

Nickel-titanium alloys (NiTi), with a matrix associated with the equiatomic intermetallic composition, are widely used among metallic alloys that exhibit shape memory effect (SME) and superelasticity (SE), due to their excellent durability, shape recovery ability, and corrosion resistance [1]. Traditionally, the industrial process of manufacturing these alloys involves four basic steps: melting and casting, hot and cold working, forming/memory-shaping, and heat treatment. However, additive manufacturing (AM) has gained prominence for producing complex and porous NiTi structures. Various routes have been developed using AM techniques, enabling the production of NiTi with SME and SE [2].

In the past decade, metal additive manufacturing has advanced rapidly, becoming a revolutionary technology that transforms product design across various industrial sectors. Pioneering fields such as the biomedical and aerospace industries have demonstrated that components designed through AM offer significant performance improvements. However, there is less detailed information about the microstructure and mechanical properties of metals and alloys produced in this

way. To fully explore the potential of metal AM, especially for structural parts, it is crucial to understand the anisotropy and microstructural and mechanical property heterogeneity that this process generally presents [3,4].

Selective laser melting (SLM) is an AM technique based on the melting of a pre-deposited powder bed layer by layer. Also known as an advanced form of selective laser sintering (SLS) when the energy density is not sufficient for melting. On the other hand, when this energy density is sufficient for melting, SLM allows the complete fusion of the metal powder, with distinct possibilities of densification levels, high mechanical strength, and strong texturization relative to the build direction. In SLM/SLS manufacturing, a CAD (Computer-Aided Design) model of the desired part is virtually divided into horizontal layers with thicknesses ranging from 30 to 100 μm [5-8]. During the process, a focused laser beam transmits the contour information of each layer to the metal powder bed, melting and solidifying, in the case of SLM, the material point by point as per the laser path. After scanning

¹Programa de Pós-Graduação em Ciência e Engenharia de Materiais – PPGCEM, Instituto Militar de Engenharia – IME, Rio de Janeiro, RJ, Brasil.

²Laboratoire de Mécanique Paris-Saclay, Gif-sur-Yvette, França.

³Instituto de Estudos Avançados – IEAv, São José dos Campos, SP, Brasil.

⁴Instituto Tecnológico de Aeronáutica – ITA, São José dos Campos, SP, Brasil.

*Corresponding author: danilocorrea@ime.eb.br



a layer, the build platform is lowered by the thickness of the next layer and covered with powder. This scanning and recoating cycle repeats until all layers are processed. The part is attached to the build platform via support structures and can be removed from the machine after the process is complete [8-10].

Metal AM has the potential to revolutionize the design and construction of metal parts in the digital industrial age. In recent years, sales of additive systems for metals have increased significantly, and the technologies have matured for industrial applications. Consequently, research interest in this area has grown exponentially, especially in the last five years [5,8,10]. However, the additive manufacturing of NiTi alloy to achieve SME and SE is still under development, particularly concerning the use of elemental powder mixtures of nickel (Ni) and titanium (Ti). Previous studies have highlighted the practical difficulties in determining the parameters necessary to produce NiTi alloy from elemental HDH Ti (hydrogenated-dehydrogenated) and Ni obtained by oxidation and reduction reaction, in order to obtain a highly densified part, free of cracks and significant residual fractions of pure Ni and Ti in the microstructure. Moreover, the strong exothermic reaction due to the formation of Ni_xTi_y intermetallics, which occurs during AM with a laser, can disturb the melt pool, making it difficult to achieve the desired phases through SLM [11].

Instrumented ultramicrohardness equipment, with depth-sensing capabilities, is widely used to evaluate the hardness and Young's modulus of materials.

The depth resolution of this technique enables the use of ultra-low loads. In this regard, it is possible to assess the dynamic hardness as a function of depth in thin coatings deposited by electrodeposition [12], as well as the microhardness and residual stress in mechanically treated surfaces by ball burnishing [13].

This technique also allows for the monitoring of the dynamic recrystallization phenomenon in elastocaloric alloys [14] and the development of thermomechanical treatments in NiTi alloys [15]. Current advancements in hardness testing instrumentation aim to provide three-dimensional observation of mechanical properties [16].

This study aims to evaluate certain mechanical properties obtained through instrumented ultramicrohardness testing of NiTi alloy produced via additive manufacturing, using the SLM technique from a powder bed composed of a mixture of elemental Ni powders, obtained by oxidation and reduction reaction, and HDH Ti.

2 Materials and methods

Ultramicrohardness tests were conducted on NiTi samples fabricated via SLM from elemental powders of Ni and HDH Ti, following the work of Gonçalves [17], which explored the laser remelting procedure. In the SLM process for most of the samples studied, two laser passes were applied to each layer, as observed in literature studies [18]: the first with lower energy to initiate the interaction and fusion between the particles, and the second with higher power to promote microstructural homogenization and layer uniformity. The SLM processes were carried out at Omnitek Tecnologia Ltda using an OmniSint-160 machine.

Additionally, as a control, a single-laser-scan per layer SLM processing condition was conducted with an energy density of 44 J/mm³, in the range corresponding to the best results obtained by Oliveira's work [11], using the same elemental powders. Based on this, the synthesis of the processing parameters adopted is described in Table 1, noting that the digits before the "/" in energy density refer to the first scan per layer, and the second pair of digits refer to the second scan per layer.

The surfaces tested in the instrumented ultramicrohardness were those corresponding to the top of the 8 mm test specimens, i.e., the cross-section, which underwent metallographic preparation, with indentations concentrated in the central region.

The instrumented ultramicrohardness tester used was the Shimadzu DUH-211S, installed at the Institute of Exact Sciences at the Fluminense Federal University (ICEx-UFF), Volta Redonda - RJ, with a Vickers pyramidal indenter at a 136° angle. From preliminary tests, a load of 100 gf (980.665 mN) produced the most appropriate indentation dimension for diagonal measurement. The loading/unloading speed was 1.0 gf/s (70.0670 mN/s), which is the standard configuration of the equipment, without holding time at the maximum load. Five indentations were performed, distributed randomly.

The basic representation of the curve generated by the instrumented ultramicrohardness test, and the main measured points, are shown in Figure 1. The measurement of the instrumented indentation, among the various available test modes, comprises a cycle that encompasses the loading and unloading phases.

Among the key parameters are the maximum penetration depth (h_{max}), the maximum load (F_{max}), and the final depth after unloading, designated as permanent indentation (h_p), manifested

Table 1. Main parameters in the production of NiTi samples by SLM

Energy Density (J/mm ³)	Melting Laser Power (W)	Remelting Laser Power (W)	Scanning Speed (mm/s)
44*	120	-	1263
30/45	60	90	1100
33/50	60	90	1000
37/55	60	90	900

* single scan per layer.

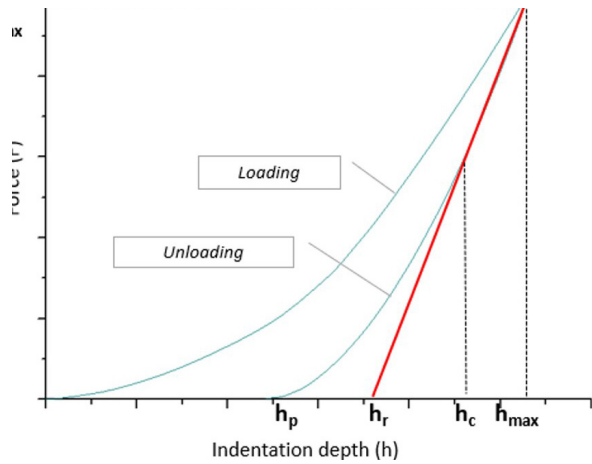


Figure 1. Representation of the applied load curve versus indentation depth of an instrumented ultramicrohardness test.

after complete load removal. The contact depth (h_c) is also considered, which corresponds to the distance at which the indenter is in actual contact with the test surface, and the elastic recovery depth (h_r), obtained by the intersection of the tangent line to the unloading curve starting from the maximum load.

For the determination of conventional Vickers hardness (HV), the calculation involves dividing the maximum applied load by the average of the two measured diagonals of the indentation. Using the force (F) in newtons and the diagonal average (d) in millimeters, a dimensional correction numerical constant is applied, as shown in Equation 1 [19].

$$HV = 0,1891 \frac{F(N)}{d^2(mm)} \quad (1)$$

Dynamic elastoplastic Vickers hardness (DHV-1), Equation 2, associates the maximum load of the test with the ratio of the maximum indentation depth (h_{max}) multiplied by the numerical constant related to the indenter's shape factor. Similarly, dynamic plastic Vickers hardness (DHV-2) can be obtained as a function of F_{max} and the indentation depth related to perfect elastic recovery (h_r), through Equation 3 [20].

$$DHV - 1 = 3,8584 \frac{F_{max}}{h_{max}^2} \quad (2)$$

$$DHV - 2 = 3,8584 \frac{F_{max}}{h_r^2} \quad (3)$$

It is also possible to derive the elastic modulus from the relationship between force and depth during indentation. The indentation modulus (E_{it}) is graphically determined by the slope of the tangent line shown in Figure 1. Mathematically, it is expressed by Equation 4 [20].

$$\frac{1}{E_r} = \frac{1 - \nu_s^2}{E_{it}} + \frac{1 - \nu_i^2}{E_i} \quad (4)$$

Where:

E_{it} – Indentation modulus

E_r – Elastic modulus converted based on indentation contact

E_i – Elastic modulus of the indenter

ν_i – Poisson's ratio of the indenter

ν_s – Poisson's ratio of the sample

3 Results and discussion

Figure 2 presents the loading and unloading curves from the ultramicrohardness test with a maximum load of 98.066 mN (100 gf) for the four samples described in Table 1. In general, the curves exhibited similar characteristics for the five measurements taken at central region of the sample, as there was no significant variation in the positioning or behavior of the curves. However, the sample with 44 J/mm³ showed greater variability compared to the others. This observation considers both the dispersion in the positioning of the five curves and the slope of the loading and unloading curves, maximum indentation depth, and permanent indentation depth.

Figure 3 shows the results for dynamic elastoplastic Vickers hardness (DHV-1) and dynamic plastic Vickers hardness (DHV-2). Numerically, the average DHV-2 values were higher than DHV-1 in all test groups, as dynamic elastoplastic hardness considers the depth of the indentation associated with both elastic and plastic deformations. The maximum indentation depth (h_{max}), used to calculate DHV-1 according to Equation 2, is greater than the indentation depth related to perfect elastic recovery (h_r), used to calculate DHV-2 in Equation 3.

This results in higher DHV-2 values compared to DHV-1 for the same measurement point in the instrumented ultramicrohardness test on a given sample.

The graph in Figure 4 presents the results of conventional Vickers hardness (HV) and the indentation modulus (E_{it}). At first glance, there is no significant difference in HV between the 30/45 and 33/50 J/mm³ samples when observing their average values. However, the 33/50 J/mm³ results show greater dispersion compared to 30/45 J/mm³ and the other samples (44 and 37/55 J/mm³). Additionally, the 44 J/mm³ result lies in an intermediate range between the 30/45 J/mm³ and 37/55 J/mm³ samples, including when observing the range of dispersion for both results.

Thus, when observing only the group of samples that underwent remelting, there is a tendency for hardness to decrease with increasing energy density, especially concerning the dynamic hardness values DHV-1 and DHV-2 (Figure 3) compared to HV (Figure 4).

Silva et. al. [14], in their study on the dynamic recrystallization of the Ti₄₆Ni₃₈Cu₁₀Nb₆ alloy, also observed high dispersion in the dynamic hardness and indentation modulus results. Rodrigues et al. [15] reported hardness values ranging from 200 to 300 HV in solution-treated NiTi samples. The higher values found in this work account for

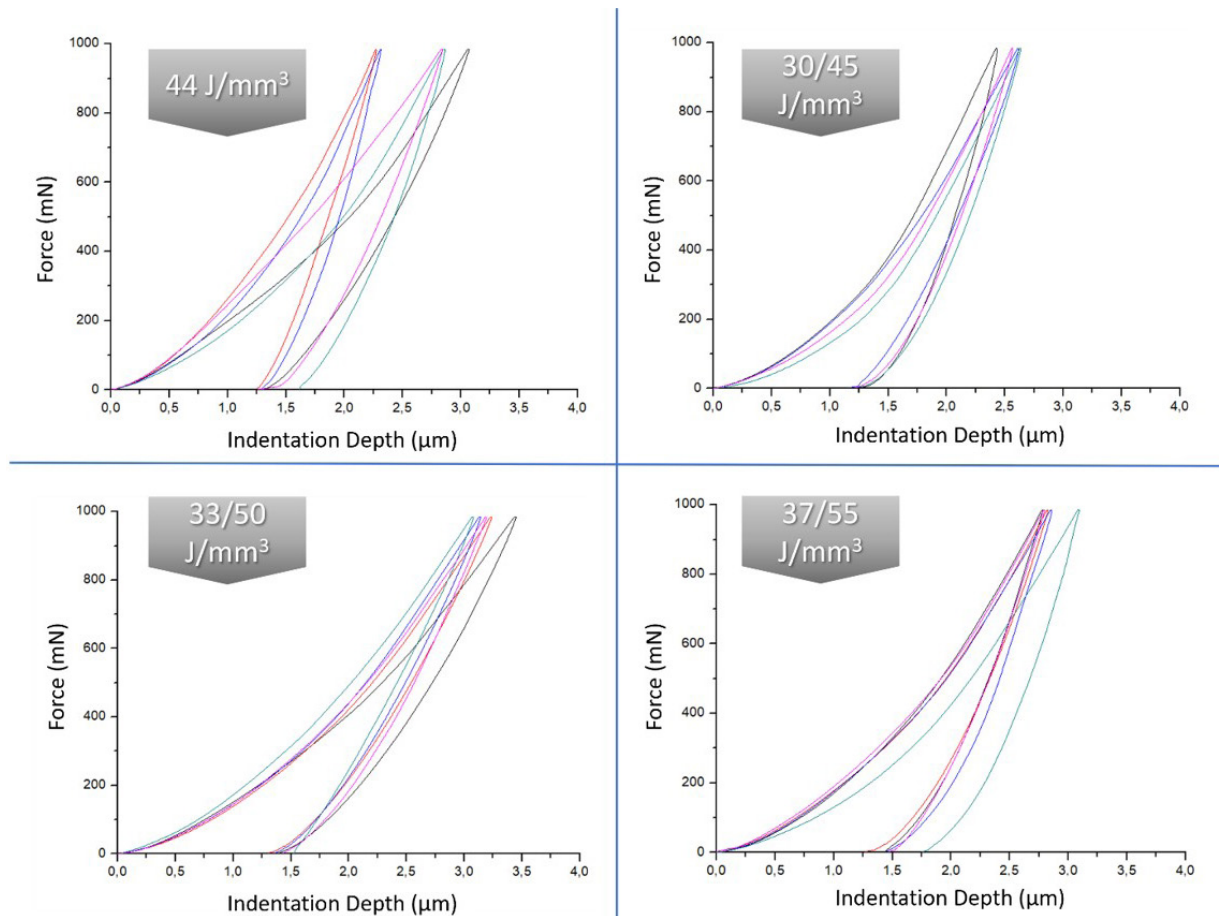


Figure 2. Applied load versus indentation depth curve for the samples: 44, 30/45, 33/50, and 37/55 J/mm³.

residual stresses and microstructural heterogeneities, which are typical of SLM fabrication.

In Gonçalves' study [17], X-ray diffraction and electron backscatter diffraction (EBSD) analysis in a scanning electron microscope with a field emission gun (FEG) were conducted on the samples in this study, highlighting non-equiatomic intermetallic phases (Ni_xTi_y) from the Ni-Ti system alongside the equiatomic NiTi intermetallic in its various structures (B2, B19', and R phases), which were observed. In that study, it was evident that the presence of precipitates, particularly Ni_3Ti (1071 HV), accounts for the hardness increase in the NiTi matrix, as this last phase in its austenitic B2 form has hardness around 275 HV, and in its martensitic B19' form, it presents hardness values of approximately 112 HV, respectively. Meanwhile, the Ti-rich intermetallic phase, $NiTi_2$, has a hardness of 163 HV [21,22]. On the other hand, the hardness and indentation modulus of the R phase are lower than those of the B2 phase, despite having similar elastic recovery when evaluating properties through instrumented hardness tests [23].

The lower hardness, in terms of HV, DHV-1, and DHV-2, and intermediate values with lower dispersion of E_{it} , compared to the other samples tested, found in the 37/55 J/mm³ sample, is an indication of microstructural

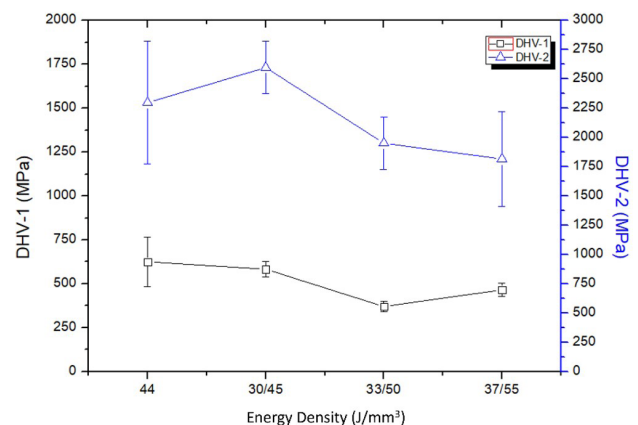


Figure 3. Results of dynamic elastoplastic Vickers hardness (DHV-1) and dynamic plastic Vickers hardness (DHV-2).

homogeneity in the cross-section relative to the build direction of the samples in disc format.

The indentation modulus is related to the elastic stiffness of the tested region, meaning the lower the value, the greater the elastic recovery capacity of the present phases. Likewise, greater recovery of shape/phase

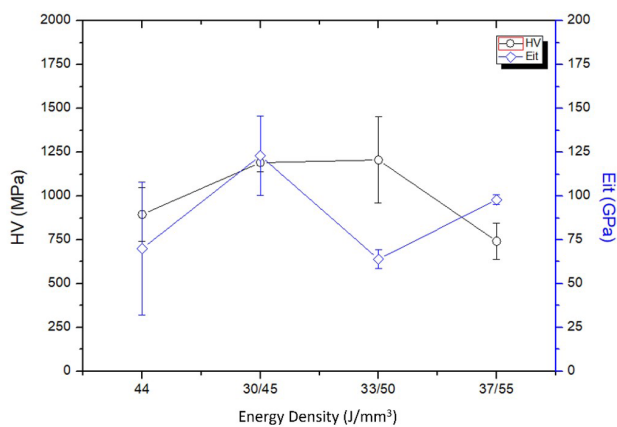


Figure 4. Results of Vickers hardness (HV) and indentation modulus (E_{it}).

transformation reversal in the case of B2 or R phases occurs when subjected to mechanical stress without dislocation movement. Although the E_{it} results are within the same range for the four samples, when considering the results in terms of their dispersion, the higher the power applied during the remelting pass (second scan), the lower the dispersion. It is noteworthy that E_{it} values near 100 GPa for the 37/55 J/mm³ sample and around 60-70 GPa for the 33/55 J/mm³ sample are very close to the results observed by Domashenkov et al. [23] when analyzing the B2 and R phases, respectively.

Akbarpour et al. [21], for an alloy composed mainly of NiTi-B2 and Ni₃Ti, with smaller amounts of NiTi-B19' and NiTi₂, achieved hardness of 750 HV, similar to that observed in this work. This justifies the high hardness values of the tested samples and the lower dispersion of indentation modulus results.

4 Conclusion

Based on the ultramicrohardness tests conducted, the loading and unloading curves showed similar patterns across

the samples, except for the sample with 44 J/mm³, which demonstrated greater variation. The analysis of dynamic elastoplastic hardness (DHV-1) and dynamic plastic hardness (DHV-2) revealed that DHV-2 exhibited higher average values than DHV-1 in all tested groups. Additionally, the Vickers hardness (HV) and indentation modulus (E_{it}) showed a trend of decreasing hardness with increasing energy density in the samples that underwent remelting.

The mechanical behavior, in terms of increasing hardness in the NiTi matrix, was attributed to the presence of precipitates such as Ni₃Ti, as the austenitic B2 and martensitic B19' and R phases, associated with NiTi, have lower hardness values. The 37/55 J/mm³ sample stood out for its lower hardness and lower E_{it} dispersion, indicating greater microstructural homogeneity. The indentation modulus was related to the elastic stiffness of the tested regions, being lower for samples with greater elastic recovery capacity.

The analysis of the results suggests that variations in the energy density applied during fabrication significantly affect the mechanical properties of NiTi alloys. Optimizing these parameters is critical to improving the quality and performance of parts produced via additive manufacturing, particularly for applications requiring high strength and elastic recovery.

Acknowledgements

The authors express their gratitude to IPT, São Paulo/SP – Brazil, for the production of HDH Ti powder, to Mr. Antônio Fasano, president of Omnitek Tecnologia Ltda, for the SLM processing, and to IME, Rio de Janeiro/RJ – Brazil, for access to the Electron Microscopy Laboratory resources. The master's, doctoral, and postdoctoral scholarships are associated with the CAPES Project (Process 88887.285953/2018-00 – Pró-Defesa IV Scholarship) and the CNPq research productivity scholarship PQ-2 (Process 307798/2015-1). Finally, acknowledgements to CAPES for the CAPES/PROEX resources that support research and development activities within the scope of PPGCEM/IME.

References

- 1 Nakahata T. Industrial processing of titanium–nickel (Ti–Ni) shape memory alloys (SMAs) to achieve key properties. In: Yamauchi K, editor. Shape memory and superelastic alloys. Cambridge: Elsevier; 2011. p. 53-62.
- 2 Elahinia M, Shayesteh Moghaddam N, Taheri Andani M, Amerinatanzi A, Bimber BA, Hamilton RF. Fabrication of NiTi through additive manufacturing: a review. *Progress in Materials Science*. 2016 [cited 2019 July 3];83:630-663. Available at: <https://www.sciencedirect.com/science/article/pii/S0079642516300469#s0115>.
- 3 Prakash KS, Nancharaih T, Rao VVS. Additive manufacturing techniques in manufacturing: an overview. *Materials Today: Proceedings*. 2018;5(2):3873-3882. <http://doi.org/10.1016/j.matpr.2017.11.642>.
- 4 Kok Y, Tan XP, Wang P, Nai MLS, Loh NH, Liu E, et al. Anisotropy and heterogeneity of microstructure and mechanical properties in metal additive manufacturing: a critical review. *Materials & Design*. 2018;139:565-586. <http://doi.org/10.1016/j.matdes.2017.11.021>.

- 5 Harun WSW, Kamariah MSIN, Muhamad N, Ghani SAC, Ahmad F, Mohamed Z. A review of powder additive manufacturing processes for metallic biomaterials. *Powder Technology*. 2018;327:128-151. <http://doi.org/10.1016/j.powtec.2017.12.058>.
- 6 Bormann T, Schumacher R, Müller B, Mertmann M, De Wild M. Tailoring selective laser melting process parameters for NiTi implants. *Journal of Materials Engineering and Performance*. 2012;21(12):2519-2524.
- 7 Zhang B, Chen J, Coddet C. Microstructure and transformation behavior of in-situ shape memory alloys by selective laser melting ti–ni mixed powder. *Journal of Materials Science and Technology*. 2013 [cited 2019 October 17];29(9):863-867. Available at: <https://www.sciencedirect.com/science/article/pii/S1005030213001254>
- 8 Volpato N. *Manufatura Aditiva: Tecnologia e aplicações da impressão 3D*. São Paulo: Blucher; 2017. 400 p.
- 9 Gibson I, Rosen D, Stucker B. *Additive manufacturing technologies: 3D printing, rapid prototyping, and direct digital manufacturing*, second edition. New York: Springer; 2015.
- 10 Gibson I, Rosen DW, Stucker B. *Additive manufacturing technologies: Rapid prototyping to direct digital manufacturing*. New York: Springer US; 2010.
- 11 Oliveira RV, Pereira de Lima Y, Hoisler Sallet E, Abílio Corrêa Gonçalves D, Vieira Le Sénéchal N, Alves Oliveira Melo E, et al. Production of cylindrical specimens based on the Ni-Ti system by selective laser melting from elementary powders. *Journal of Materials Engineering and Performance*. 2021;30(7):5477-5490.
- 12 Oliveira RP, Bertagnolli DC, Silva L, Ferreira EA, Paula AS, Fonseca GS. Effect of Fe and Co co-deposited separately with Zn-Ni by electrodeposition on ASTM A624 steel. *Applied Surface Science*. 2017;420:53-62.
- 13 Oliveira DA, Martins AM, Santos AJD, Castro Magalhães F, Abrão AM. Influence of the hydrostatic ball burnishing on surface quality and ultra-microhardness. *Journal of the Brazilian Society of Mechanical Sciences and Engineering*. 2024;46(2):74.
- 14 Silva JD, Santos DS, Buono VTL, Santos LA. Influence of hot rolling on microstructure, mechanical properties, and martensitic transformation of TiNiCuNb shape memory alloy. *Vacuum*. 2024;230:113751.
- 15 Rodrigues PF, Teixeira RS, Le Sénéchal NV, Fernandes FMB, Paula AS. The influence of the soaking temperature rotary forging and solution heat treatment on the structural and mechanical behavior in Ni-rich niti alloy. *Materials (Basel)*. 2022;15(1):63.
- 16 Hirooka D, Furushiro N, Yamaguchi T. Three-dimensional indentation test system for observing the distribution of internal mechanical properties in materials. *Precision Engineering*. 2024;91:143-154.
- 17 Gonçalves D. *Elaboração de liga NiTi por fusão seletiva a laser a partir dos pós de Ni de oxirredução e Ti HDH*. Rio de Janeiro: Instituto Militar de Engenharia; 2023.
- 18 Bernard A, Kruth JP, Cao J, Lanza G, Bruschi S, Merklein M, et al. Vision on metal additive manufacturing: Developments, challenges and future trends. *CIRP Journal of Manufacturing Science and Technology*. 2023;47:18-58.
- 19 ASTM. *Test Methods for Vickers Hardness and Knoop Hardness of Metallic Materials*. West Conshohocken, PA: ASTM International; 2023 [cited 2024 July 3]. Available at: <http://www.astm.org/cgi-bin/resolver.cgi?E92-23>
- 20 Shimadzu Corporation. *Manual Shimadzu DUH-211S*. Chiyoda-ku: Brochure Shimadzu Corporation; 2018.
- 21 Akbarpour MR, Alipour S, Najafi M, Ebadzadeh T, Kim HS. Microstructural characterization and enhanced hardness of nanostructured Ni₃Ti–NiTi (B2) intermetallic alloy produced by mechanical alloying and fast microwave-assisted sintering process. *Intermetallics*. 2021;131:107119.
- 22 Li YF, Tang SL, Gao YM, Ma SQ, Zheng QL, Cheng YH. Mechanical and thermodynamic properties of intermetallic compounds in the Ni–Ti system. *International Journal of Modern Physics B*. 2017;31(22):1750161.
- 23 Domashenkov A, Doubenskaia M, Smurov I, Smirnov M, Travianov A. Selective laser melting of NiTi powder. In: *Lasers in Manufacturing Conference*. Munich, Germany. Stuttgart: IFSW, 2017.

Received: 4 Oct. 2024

Accepted: 7 Jan. 2025

Editor-in-charge:

André Luiz Vasconcellos da Costa e Silva 